chemosensors

MDPI

Communication

Electrical and Humidity-Sensing Properties of $EuCl_2$, Eu_2O_3 and $EuCl_2/Eu_2O_3$ Blend Films

Pi-Guey Su * and Nok-Him Choy

Department of Chemistry, Chinese Culture University, Taipei 111, Taiwan; choynh516@gmail.com
* Correspondence: spg@ulive.pccu.edu.tw; Tel.: +886-2-2861-0511 (ext. 25332)

Abstract: Impedance-type humidity sensors based on $EuCl_2$, Eu_2O_3 and $EuCl_2/Eu_2O_3$ blend films were fabricated. The electrical properties of the pure $EuCl_2$ and Eu_2O_3 films and $EuCl_2/Eu_2O_3$ blend film that was blended with different amounts of $EuCl_2$ were investigated as functions of relative humidity. The influences of the $EuCl_2$ to the humidity-sensing properties (sensitivity and linearity) of the $EuCl_2/Eu_2O_3$ blend film were thus elucidated. The impedance-type humidity sensor that was made of a 7 wt% $EuCl_2/Eu_2O_3$ blend film exhibited the highest sensitivity, best linearity, a small hysteresis, a fast response time, a small temperature coefficient and long-term stability. The complex impedance plots were used to elucidate the role of ions in the humidity-sensing behavior of the $EuCl_2/Eu_2O_3$ blend film.

Keywords: humidity sensor; $EuCl_2$; Eu_2O_3; $EuCl_2/Eu_2O_3$ blend film; complex impedance plots

check for updates

Citation: Su, P.-G.; Choy, N.-H. Electrical and Humidity-Sensing Properties of $EuCl_2$, Eu_2O_3 and $EuCl_2/Eu_2O_3$ Blend Films. *Chemosensors* **2021**, *9*, 288. https://doi.org/10.3390/chemosensors9100288

Academic Editor: Bilge Saruhan-Brings

Received: 12 September 2021
Accepted: 7 October 2021
Published: 11 October 2021

1. Introduction

Developing humidity sensors have attracted much interest because humidity is an important role in maintaining human health and an excellent quality of products [1–3]. Therefore, humidity sensors must have high sensitivity, a wide working humidity range, good linearity, fast response/recovery times, low hysteresis, good reversibility, stability and ease of fabrication for the mass production of humidity devices for using in food storage, industrial production and environmental monitoring [4,5]. Many materials, including ceramic, polyelectrolyte, organic polymer and composite materials, have been applied to humidity sensors [1,6–14]. Ceramic materials, including metal oxides, perovskite- and spinel-type oxides and their hybrid systems, have some superiority in function because of their good chemical stability, high heat resistance, good water resistance under high humidity, cost-effectiveness and fast response to the changes of humidity [7,15], which means they can be applied to humidity detection. The humidity-sensing properties of ceramic humidity sensors is strongly influenced by the surface activity and the porous structure of the ceramic materials [15]. Therefore, many reports focused on researching the microstructure and morphology of ceramic materials and doping various dopants to tune the physico-chemical properties of ceramic materials [6,16].

The rare earth elements (i.e., lanthanides) could be considered as active cocatalysts and dopants for the improvement of new substances with appealing gas-sensing applications because of their 7f orbitals awarding special electronic properties [17–25]. Zhong et al. [17] fabricated Eu_2O_3-doped In_2O_3 using the sol-gel method for detecting H_2S gas. Stănoiu et al. [18] fabricated ZnO–Eu_2O_3 binary oxide for sensing NO_2 gas under humid condition. Wang et al. [19] fabricated Eu-doped SnO_2 nanofibers for sensing acetone gas. Ortega et al. [20] fabricated Eu_2O_3-doped CeO_2 for sensing CO gas. Er et al. [21] fabricated rare earth metals (Y, Ru and Cs)-doped ZnO thin films for sensing NH_3 gas at room temperature. Jing et al. [22] fabricated a PANI/Eu^{3+} nanofiber for sensing NH_3 gas. Costello et al. [23] fabricated Eu^{3+} ion-doped ZrO_2 for sensing volatile organic compounds (VOCs). Mokoena et al. [24] fabricated Eu^{3+} ion-doped NiO for sensing toluene gas. Shen et al. [25] fabricated Ce-doped ZnO nanowires for sensing ethanol. Zhang et al. [26] fabricated a humidity sensor that was made of Eu-doped ZnO using the sol-gel method. Most literatures tend to explore the effects of rare earth ions and oxides doping on the enhancing gas-sensing properties. Recently, Wang et al. [27] fabricated a fast response humidity sensor that was made of CeO_2 nanowires. However, no attempt has been used for fabricating an impedance-type humidity sensor that was made of pure $EuCl_2$, Eu_2O_3 and $EuCl_2/Eu_2O_3$ blend films. In this work, the impedance-type humidity sensors that were made of the $EuCl_2$, Eu_2O_3 and $EuCl_2/Eu_2O_3$ blend films were fabricated. The characterization of the $EuCl_2$, Eu_2O_3 and $EuCl_2/Eu_2O_3$ blend films were studied using scanning electron microscopy (SEM) and X-ray diffraction (XRD). The humidity-sensing characteristics of the $EuCl_2$, Eu_2O_3 and $EuCl_2/Eu_2O_3$ blend films, including the response, linearity, hysteresis, response/recovery times, influence of ambient temperature, influence of applied frequency and stability, were studied. The complex impedance spectra were used to investigate the humidity-sensing mechanism of the $EuCl_2/Eu_2O_3$ blend film.

2. Experimental Methods

2.1. Materials and Humidity Sensors Preparation

Europium dichloride ($EuCl_2$, 99%, Sigma-Aldrich, St. Louis, MO, USA) was used as received without further purification. The fabrication method of europium oxide (Eu_2O_3) was the thermal decomposition technique that was described in the literature [28]. The starting material was $EuCl_2$ and the decomposition temperature was 600 °C for 5 h under the ambient atmosphere in furnace. The x wt% $EuCl_2$ with 2, 5, 6, 7 and 8%wt/Eu_2O_3 blends were prepared using a wet-blending process. The Eu_2O_3 particles were impregnated with aqueous solutions of various x wt% $EuCl_2$ solutions under ultrasonicating for 1 h to achieve a homogeneous dispersion of the Eu_2O_3 particles. Figure 1a shows the structure of an impedance-type humidity sensor. The interdigitated Au electrodes were made on an alumina substrate using a screen-printing method. The gap size and line width of the Au electrode were 0.25 and 0.2 mm, respectively. Then, 20 μL of the as-prepared uniformly $EuCl_2$, Eu_2O_3 and $EuCl_2/Eu_2O_3$ blend precursor solutions were drop-coated on an as-prepared alumina substrate using a micropipette, followed by drying at 110 °C.

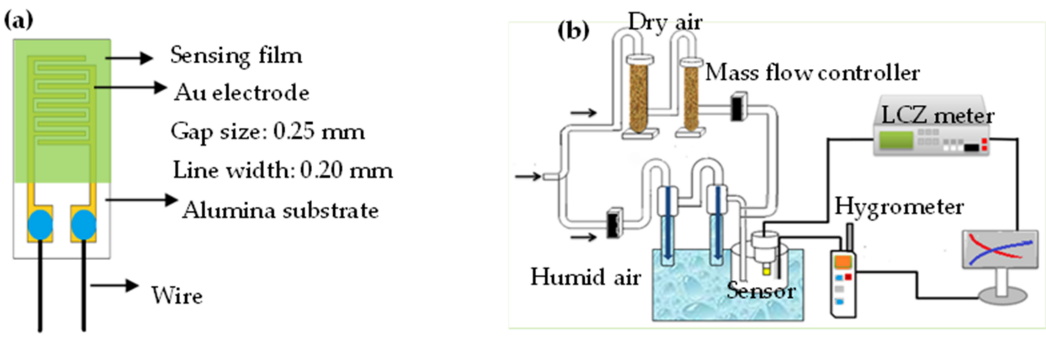

Figure 1. (**a**) structure of humidity sensor and (**b**) the impedance measurement of humidity sensors and humidity atmosphere controller.

2.2. Characterization of $EuCl_2$, Eu_2O_3 and $EuCl_2/Eu_2O_3$ Bend Films

The composition and morphologies of the $EuCl_2$, Eu_2O_3 and $EuCl_2/Eu_2O_3$ blend film was investigated using an X-ray diffraction (XRD) using Cu K_α radiation (Shimadzu, Lab XRD-6000, Taipei, Taiwan) and a scanning electron microscope (SEM, Hitachi, TM400 Plus, Tokyo, Japan).

2.3. Measurement of Electrical and Humidity-Sensing Properties

Figure 1b shows the electrical and humidity-sensing measurement system. The generation of required humidity conditions for testing sensors was controlled using a divided humidity generator system in a temperature-controlled testing chamber. The principal apparatus for controlling the generation of humidity was a divided humidity generator, in which the proportion of dry and humid air under a total flow rate was 10 L/min to obtain the required humidity conditions for testing. The carrier gas was dry air. The relative humidity (RH) values were determined using the displayed readings of a standard humidity hygrometer (with an accuracy of ±0.1% RH). The electronic properties (impedance) of the as-prepared humidity sensors vs. RH were measured using an LCZ meter.

3. Results and Discussion

3.1. Characteristics of $EuCl_2$, Eu_2O_3 and $EuCl_2/Eu_2O_3$ Blend Films

XRD Characterization and Morphology Observations

Figure 2a shows the XRD of $EuCl_2$, the peaks appearing at 2θ = 23.1°, 26.1°, 29.4°, 32.1°, 35.6°, 38.1°, 39.6°, 41.2°, 47.8°, 50.9°, 60.9° and 64.9°corresponded to the (210), (111), (211), (121), (301), (002), (230), (131), (212), (331), (232) and (610) planes of the orthorhombic structure of $EuCl_2$ [29]. Figure 2b shows the XRD spectrum of the Eu_2O_3 film that was made of the thermal decomposition of the $EuCl_2$. The peaks appearing at 2θ = 28.5°, 38.0°, 42.4°, 47.3°, 56.0° and 77.0°corresponded to the (222), (332), (431), (440), (622) and (662) planes of the body-centered cubic (BCC) structure of Eu_2O_3, indicating the formation of Eu_2O_3 crystals [30,31]. Additionally, a very similar XRD spectrum has been reported for Eu_2O_3 prepared by using a solution method [31]. Figure 2c shows the XRD of the $EuCl_2/Eu_2O_3$ blend; the peaks show it had mixed phases of $EuCl_2$ and Eu_2O_3 and no noticeable peak shifts were observed.

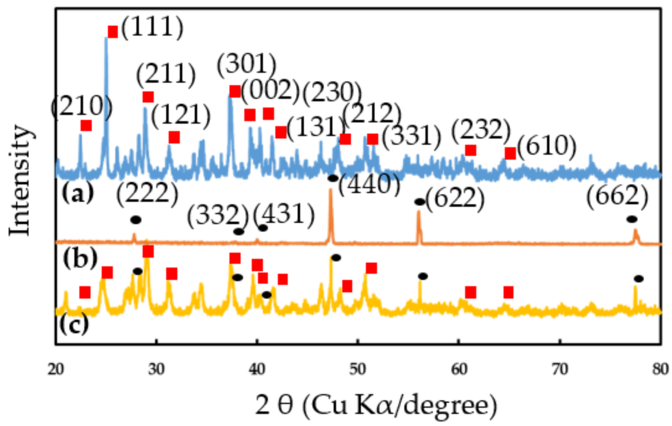

Figure 2. XRD patterns of (**a**) $EuCl_2$, (**b**) Eu_2O_3 and (**c**) $EuCl_2/Eu_2O_3$ blend films.

Figure 3 shows the morphology of the $EuCl_2$, Eu_2O_3 and $EuCl_2/Eu_2O_3$ blend films that were analyzed using scanning electron microscopy. Figure 3a shows the $EuCl_2$ film that had various unfixed shapes of a massive lamination structure. Figure 3b shows the Eu_2O_3 film, the Eu_2O_3 particles obviously aggregated to form a tight surface morphology. Figure 3c shows the 7 wt% $EuCl_2/Eu_2O_3$ blend film in a low-magnification image; this film had smoother surfaces than the Eu_2O_3 film did and many cracks in its surface. Figure 3d shows a high-magnification image of Figure 3c; the film exhibited porous structures marked by white arrows.

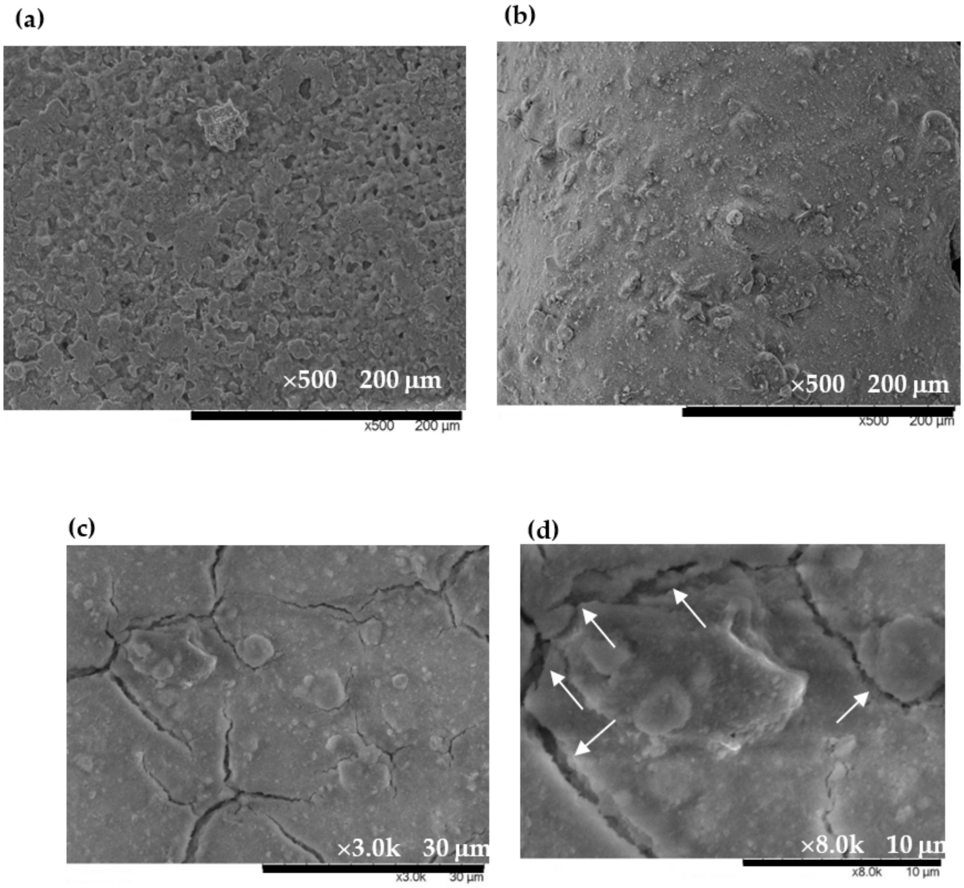

Figure 3. SEM micrographs of (**a**) $EuCl_2$ film, (**b**) Eu_2O_3 film, (**c**) 7 wt% $EuCl_2/Eu_2O_3$ blend film and (**d**) high-magnification image of $EuCl_2/Eu_2O_3$ blend film.

3.2. Electrical and Humidity-Sensing Properties of Humidity Sensors Based on $EuCl_2$, Eu_2O_3 and $EuCl_2/Eu_2O_3$ Blend Films

Figure 4 plots the log-impedance of the $EuCl_2$, Eu_2O_3 and $EuCl_2/Eu_2O_3$ blend films as a function of the relative humidity. Table 1 presents the results of the sensitivity and linearity of humidity sensing. The sensitivity and linearity were calculated as the slope and R-squared value (R^2) of the linear fitting curve in the humidity range from 20 to 90% RH, respectively. The $EuCl_2$ film exhibited a steep decrease in impedance as the RH changed from 20 to 40% RH, and very slowly decreased in the range of 40–90% RH. This result was related to the fact that $EuCl_2$ is very moisture sensitive [28]. The Eu_2O_3 film had one less order changed in impedance, with the humidity ranging from 40 to 90% RH and almost no impedance changed in the range of 20–40% RH because of its weak water adsorption and low-conduction properties. For obtaining the higher sensitivity and better linearity of the Eu_2O_3 film in a wider humidity range, a $EuCl_2/Eu_2O_3$ blend film was fabricated, and the optimum ratio of $EuCl_2$ to Eu_2O_3 was studied. The impedance of all the $EuCl_2/Eu_2O_3$ blend films continuously decreased along with the humidity increase in the range of 20–40% RH, suggesting that the strong water adsorption capacity of $EuCl_2$ improved the sensitivity of the $EuCl_2/Eu_2O_3$ blend film. The sensitivity (slope) of the 7 wt% $EuCl_2/Eu_2O_3$ blend film was greater than those of the 2, 5, 6 and 8 wt% $EuCl_2/Eu_2O_3$ blend films in the studied range (20 to 90% RH). This result was related to the fact that the blended amounts of $EuCl_2$ increased, which increased the water adsorption capacity for physisorption and chemisorption layers on the $EuCl_2/Eu_2O_3$ blend film with the humidity ranging from 40 to 90% RH. Additionally, the 7 wt% $EuCl_2/Eu_2O_3$ blend film had better linearity than that of the 8 wt% $EuCl_2/Eu_2O_3$ blend film because the impedance of the 8 wt% $EuCl_2/Eu_2O_3$ blend film slightly changed in the range of 40–90% RH. The 7 wt% $EuCl_2/Eu_2O_3$ blend film exhibited the highest response and best linearity; therefore, it was further tested to investigate its humidity-sensing properties and mechanism.

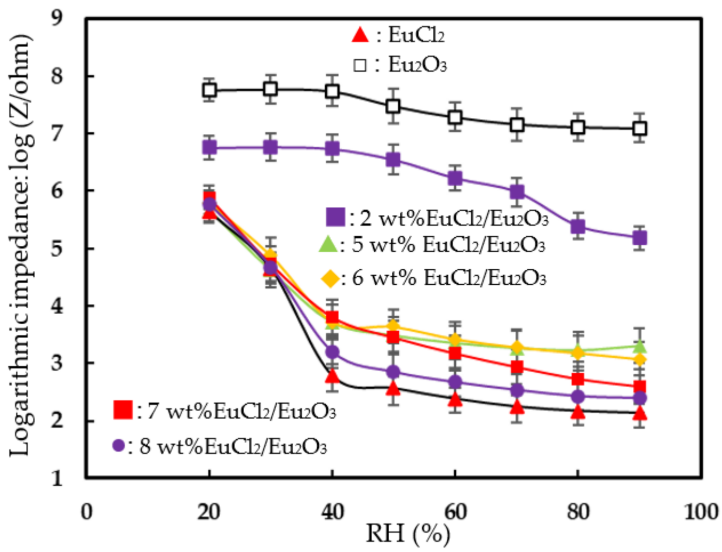

Figure 4. Log-impedance vs. relative humidity for humidity sensors based on $EuCl_2$, Eu_2O_3 and $EuCl_2/Eu_2O_3$ blend films. Measurements were made at 25 °C, 1 V AC voltage and 1 kHz frequency.

Table 1. Sensitivity and linearity of impedance-type humidity sensors based on $EuCl_2$, Eu_2O_3 and $EuCl_2/Eu_2O_3$ blend films.

Materials	Linear Fitting Curve	Sensitivity [a] (log Z/% RH)	Linearity [b] (R^2)
$EuCl_2$	Y = −0461 X + 5.612	−0.0461	0.7267
Eu_2O_3	Y = −0118 X + 8.072	−0.0118	0.9230
2 wt% $EuCl_2/Eu_2O_3$	Y = −0245 X + 7.546	−0.0245	0.8983
5 wt% $EuCl_2/Eu_2O_3$	Y = −0296 X + 5.464	−0.0296	0.6983
6 wt% $EuCl_2/Eu_2O_3$	Y = −0346 X + 5.782	−0.0346	0.7797
7 wt% $EuCl_2/Eu_2O_3$	Y = −0427 X + 6.015	−0.0427	0.8601
8 wt% $EuCl_2/Eu_2O_3$	Y = −0411 X + 5.741	−0.0411	0.7582

[a] Sensitivity is defined as the slope of the linear fitting curve from 20 to 90% RH. [b] Linearity is defined as the R-squared value (correlation coefficient) of the linear fitting curve from 20 to 90% RH.

Figure 5a shows the hysteresis of the 7 wt% $EuCl_2/Eu_2O_3$ blend film. The average hysteresis was below 1.1% RH as the humidity ranged from 20 to 90% RH in a desiccation-to-humidification cycle. The reversibility was investigated with the hysteresis of testing a desiccation-to-humidification cycle at 60% RH three times. The reversibility was 1.07% RH. Figure 5b shows the influence of ambient temperature on the impedance of the 7 wt% $EuCl_2/Eu_2O_3$ blend film vs. RH. The average temperature coefficient was about −0.10% RH/°C. Figure 5c shows the response/recovery times of the 7 wt% $EuCl_2/Eu_2O_3$ blend film. The response/recovery times were 40/80 s. The response/recovery times of the $EuCl_2$ film were 30/140 s. The 7 wt% $EuCl_2/Eu_2O_3$ blend film had faster response/recovery times than that of the $EuCl_2$ film. This result was related to the strong water adsorption capacity of $EuCl_2$. Figure 5d shows the influence of the applied frequency on the impedance of the 7 wt% $EuCl_2/Eu_2O_3$ blend film vs. RH. The applied frequency affected the impedance at low humidity more significantly (<40% RH) than that at high humidity. Figure 5e plots the long-term stability of the 7 wt% $EuCl_2/Eu_2O_3$ blend film. At testing points of 20, 60 and 90% RH, no obvious deviations in impedance were found within 53 days. The repeatability, on the same day, was performed by repeating testing at 60% RH three times and analyzed with relative standard deviation (RSD). The repeatability (RSD) was 6.3%. The humidity-sensing properties of this study were compared with those humidity sensors that were made of ceramic materials in the literature [31–33], as shown in Table 2. The present humidity sensor that was made of the 7 wt% $EuCl_2/Eu_2O_3$ blend film using a simple thermal decomposition technique had a wide humidity-sensing range, a comparable sensitivity and low hysteresis compared to the humidity sensors that were made of Li^+ and K^+ ions-doped ZnO, SnO_2 and TiO_2.

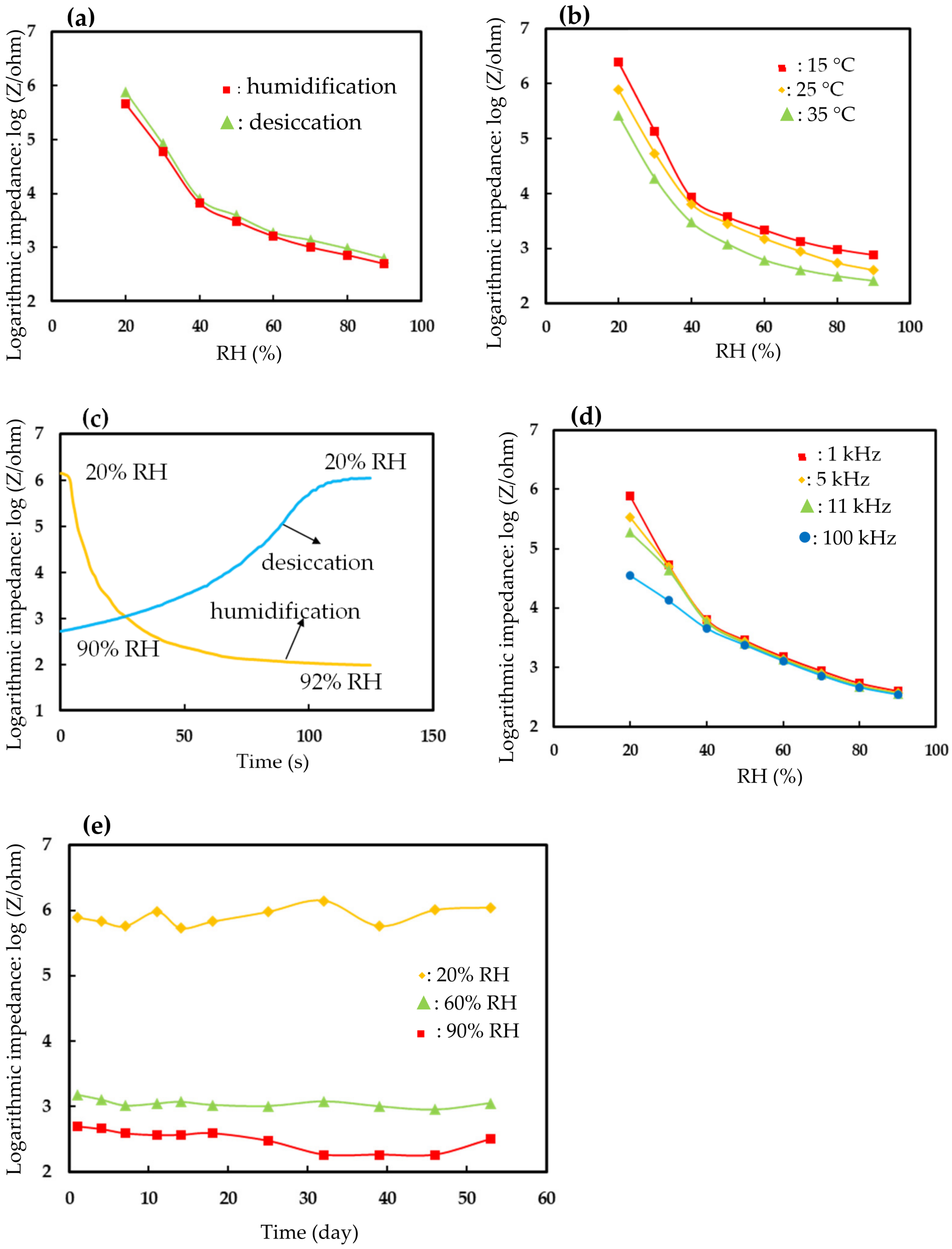

Figure 5. Humidity-sensing properties of the humidity sensor based on 7 wt% $EuCl_2/Eu_2O_3$ blend film. (**a**) Hysteresis, (**b**) effect of ambient temperature, (**c**) response/recovery times, (**d**) effect of applied frequency, (**e**) long-term stability.

Table 2. Humidity sensor performance of this work compared with the humidity sensors based on ceramic materials in the literatures.

Sensing Material	Working Range (% RH)	Sensitivity	Hysteresis (% RH)	Response Time (s)	Ref.
LiCl-doped TiO_2	13–65	—	—	0.5	[32]
LiCl-doped ZnO	11–95	—	2	3	[33]
KCl-doped SnO_2	11–95	4 order [a]	—	5	[34]
$EuCl_2$-blended Eu_2O_3	20–90	0.0427 [b]	<1.1	40	This work

[a] Sensitivity is defined as order in impedance cganges over entire testing humidity range. [b] Sensitivity is defined as slope (−(log Z/% RH)) of the linesr fitting curve over entire testing humidity range.

3.3. Humidity-Sensing Mechanism

The complex impedance spectrum was useful for studying the conduction mechanisms of humidity sensors. Figure 6 shows the measured impedance spectra of the humidity sensor that was made of the 7 wt% $EuCl_2/Eu_2O_3$ blend film. At low humidity (20% RH), a semicircular plot of the film impedance was obtained. The semicircle plot of the impedance has been explained by many authors [35–37], resulting mainly from the intrinsic impedance of the 7 wt% $EuCl_2/Eu_2O_3$ blend film, and the film could be modeled as an equivalent parallel circuit that incorporates a resistor and a capacitor. When increasing the RH (40, 50 and 60%), the semicircle radius gradually reduced and a straight line appeared at low frequencies. The straight line represented Warburg impedance, which was caused by the diffusion of H_3O^+ ions across the interface between the electrode and the sensing film [35]. Finally, when increasing the RH to 80%, the semicircle disappeared and only a straight line was observed. These results were related to the fact that, upon the adsorption of water, the adsorbed water molecules on the 7 wt% $EuCl_2/Eu_2O_3$ blend film formed a thin liquid layer, and resultingly, gradually dissociated to form H_3O^+ ions. At high RH, the sorbed water acted as a plasticizer, increasing the mobility of the solvated H_3O^+ ions diffusing across the interface between the electrode and the liquid-like 7 wt% $EuCl_2/Eu_2O_3$ blend film. According to the obtained complex impedance plots, the humidity-sensing by the 7 wt% $EuCl_2/Eu_2O_3$ blend film depended on the H_3O^+ ion transport mechanism [37,38].

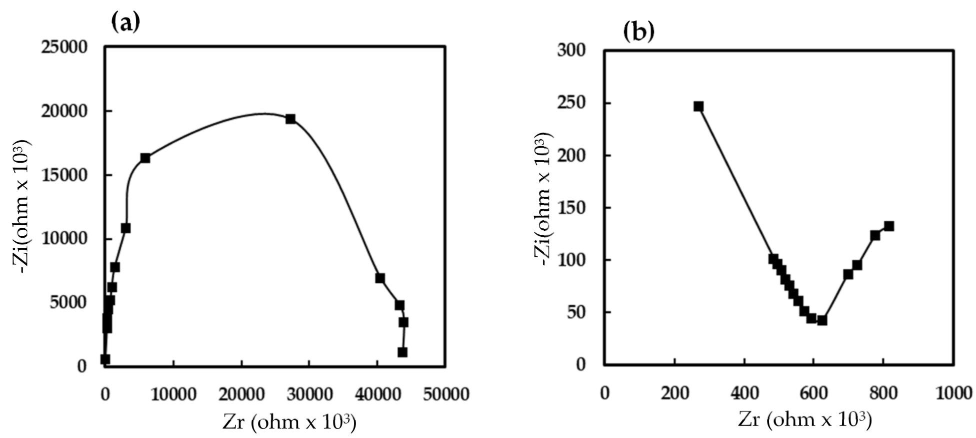

Figure 6. *Cont.*

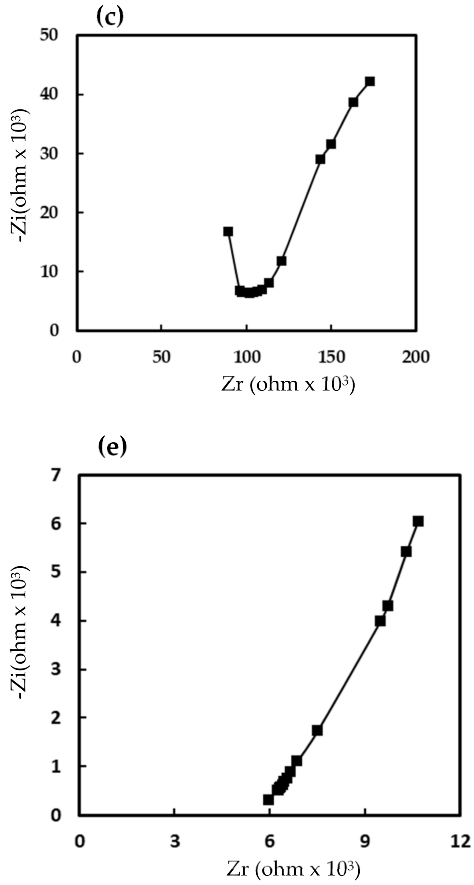

Figure 6. Complex impedance plots of humidity sensor based on 7 wt% $EuCl_2/Eu_2O_3$ blend film at (**a**) 20% RH, (**b**) 40% RH, (**c**) 50% RH, (**d**) 60% RH and (**e**) 80% RH. Measurements were made at frequency ranging from 50 to 100,000 Hz, RH ranging from 20 to 80% RH, at 1 V AC voltage and at 25 °C.

4. Conclusions

The humidity sensor based on the $EuCl_2$ film was well suited to low humidity (20–40% RH) because of its strong water adsorption property. The humidity sensor based on the Eu_2O_3 film exhibited a small humidity-working range (40~90% RH) because of its weak water adsorption and low-conduction properties. The humidity sensor based on the $EuCl_2/Eu_2O_3$ blend film exhibited high sensitivity and good linearity over the entire RH range (20 to 90% RH) because of the added $EuCl_2$ to increase the water adsorption and conductance of the $EuCl_2/Eu_2O_3$ blend film. The impedance-type humidity sensor that was made of the 7 wt% $EuCl_2/Eu_2O_3$ blend film exhibited high sensitivity (slope = 0.0427) and the best linearity (R^2 = 0.8601), small hysteresis (<1.1% RH), a small ambient temperature coefficient (−0.10% RH/ °C), fast response/recovery times (40/80 s) and good long-term stability (at least 53 days). The complex impedance plots of the $EuCl_2/Eu_2O_3$ blend film changed from semicircular to linear as the RH increased. These results reflect the H_3O^+ ions that dominated the conductance of the $EuCl_2/Eu_2O_3$ blend film.

Author Contributions: Conceptualization, P.-G.S.; methodology, P.-G.S.; investigation, P.-G.S. and N.-H.C.; writing—original draft preparation, P.-G.S.; writing—review and editing, P.-G.S.; supervision, P.-G.S.; project administration, P.-G.S.; funding acquisition, P.-G.S. All authors have read and agreed to the published version of the manuscript.

Funding: This research was founded by Ministry of Science and Technology of Taiwan, grant no. MOST 110-2113-M-034-002.

Institutional Review Board Statement: Not applicable.

Informed Consent Statement: Not applicable.

Data Availability Statement: Not applicable.

Conflicts of Interest: The authors declare no conflict of interest.

References

1. Sakai, Y.; Sadaoka, Y.; Matsuguchi, M. Humidity sensors based on polymer thin films. *Sens. Actuators B* **1996**, *35–36*, 85–90. [CrossRef]
2. Luo, Y.; Kun, Y.; Shi, Y.; Shang, C. Research of radiosonde humidity sensor with temperature compensation function and experimental verification. *Sens. Actuators A* **2014**, *218*, 49–59. [CrossRef]
3. Lee, S.W.; Choi, B.I.; Kim, J.C.; Woo, S.B.; Kim, Y.G.; Yoo, J.; Seo, Y.S. Reduction and compensation of humidity measurement errors at cold temperatures using dual QCM humidity sensors based on graphene oxides. *Sens. Actuators B* **2019**, *284*, 386–394. [CrossRef]
4. Farahani, H.; Wagiran, R.; Hamidon, M.N. Humidity sensors principle, mechanism, and fabrication technologies: A comprehensive review. *Sensors* **2014**, *14*, 7881–7939. [CrossRef]
5. Najeeb, M.A.; Ahmad, Z.; Shakoor, R.A. Organic thin-film capacitive and resistive humidity sensors: A focus review. *Adv. Mater. Interfaces* **2018**, *5*, 1–19. [CrossRef]
6. Blank, T.A.; Eksperiandova, L.P.; Belikov, K.N. Recent trends of ceramic humidity sensors development: A review. *Sens. Actuators B* **2016**, *228*, 416–442. [CrossRef]
7. Zhang, D.; Tong, J.; Xia, B.; Xue, Q. Ultrahigh performance humidity sensor based on layer-by-layer self-assembly of graphene oxide/polyelectrolyte nanocomposite film. *Sens. Actuators B* **2014**, *203*, 263–270. [CrossRef]
8. Sakai, Y.; Matsuguchi, M.; Hurukawa, T. Humidity sensor using crosslinked poly(chloromethyl styrene). *Sens. Actuators B* **2000**, *66*, 135–138. [CrossRef]
9. Zhang, D.; Sun, Y.; Li, P.; Zhang, Y. Facile fabrication of MoS_2-modified SnO_2 hybrid nanocomposite for ultrasensitive humidity sensing. *ACS Appl. Mater. Interfaces* **2016**, *8*, 14142–14149. [CrossRef]
10. Taccola, S.; Greco, F.; Zucca, A.; Innocenti, C.; de Julián Fernández, C.; Campo, G.; Sangregorio, C.; Mazzolai, B.; Mattoli, V. Characterization of free-standing PEDOT: PSS/iron oxide nanoparticle composite thin films and application as conformable humidity sensors. *ACS Appl. Mater. Interfaces* **2013**, *5*, 6324–6332. [CrossRef]
11. Zhang, D.; Tong, J.; Xia, B. Humidity-sensing properties of chemically reduced graphene oxide/polymer nanocomposite film sensor based on layer-by-layer nano self-assembly. *Sens. Actuators B* **2014**, *197*, 66–72. [CrossRef]
12. Ziegler, D.; Boschetto, F.; Marin, E.; Palmero, P.; Pezzotti, G.; Tulliani, J.M. Rice husk ash as a new humidity sensing material and its aging behavior. *Sens. Actuators B* **2021**, *328*, 129049. [CrossRef]
13. Chen, Q.; Yao, Y.; Huang, X.H.; Liu, D.; Mao, K.l. Simulation analysis and experimental verification for sensitivity of IDE-QCM humidity sensors. *Sens. Actuators B* **2021**, *341*, 129992. [CrossRef]
14. Chen, Q.; Huang, X.H.; Yao, Y.; Luo, K.B.; Pan, H.Z.; Wang, Q. Ringed electrode configuration enhances the sensitivity of QCM humidity sensor based on lignin through fringing field effect. *IEEE Sens. J.* **2021**, 3109446. [CrossRef]
15. Faia, P.M.; Furtado, C.S.; Ferreira, A.J. Humidity sensing properties of a thick-film titania prepared by a slow spinning process. *Sens. Actuators B* **2004**, *101*, 183–190. [CrossRef]
16. Bârsan, N.; Simion, C.; Heine, T.; Pokhrel, S.; Weimar, U. Modeling of sensing and transduction for p-type semiconducting metal oxide based gas sensors. *J. Electroceramics* **2010**, *25*, 11–18. [CrossRef]
17. Niu, X.; Zhong, H.; Wang, X.; Jiang, K. Sensing properties of rare earth oxide doped In_2O_3 by a sol–gel method. *Sens. Actuators B* **2006**, *115*, 434–438. [CrossRef]
18. Stănoiu, A.; Simiona, C.E.; Somăcescu, S. NO_2 sensing mechanism of ZnO–Eu_2O_3 binary oxide under humid air conditions. *Sens. Actuators B* **2013**, *186*, 687–694. [CrossRef]
19. Jiang, Z.; Zhao, R.; Sun, B.; Nie, G.; Ji, H.; Lei, J.; Wang, C. Highly sensitive acetone sensor based on Eu-doped SnO_2 electrospun nanofibers. *Ceram. Int.* **2016**, *42*, 15881–15888. [CrossRef]
20. Ortega, P.P.; Rocha, L.S.R.; Cortés, J.A.; Ramirez, M.A.; Buono, C.; Ponce, M.A.; Simões, A.Z. Towards carbon monoxide sensors based on europium doped cerium dioxide. *Appl. Surf. Sci.* **2019**, *464*, 692–699. [CrossRef]
21. Sarf, F.; Er, I.K.; Yakar, E.; Acar, S. The role of rare-earth metal (Y, Ru and Cs)-doped ZnO thin films in NH_3 gas sensing performances at room temperature. *J. Mater Sci. Mater Electron.* **2020**, *31*, 10084–10095. [CrossRef]
22. Zhang, W.; Li, G.; She, C.; Liu, A.; Cheng, J.; Li, H.; Liu, S.; Jing, C.; Cheng, Y.; Chu, J. High performance tube sensor based on PANI/Eu3+ nanofiber for low-volume NH_3 detection. *Anal. Chim. Acta* **2020**, *1093*, 115–122. [CrossRef] [PubMed]
23. Fois, M.; Cox, T.; Ratcliffe, N.; de Lacy Costello, B. Rare earth doped metal oxide sensor for the multimodal detection of volatile organic compounds (VOCs). *Sens. Actuators B* **2021**, *330*, 129264. [CrossRef]
24. Mokoena, T.P.; Swart, H.C.; Hillie, K.T.; Motaung, D.E. Engineering of rare-earth Eu_3+ ions doping on p-type NiO for selective detection of toluene gas sensing and luminescence properties. *Sens. Actuators B* **2021**, *347*, 130530. [CrossRef]
25. Zhao, S.; Shen, Y.; Li, A.; Chen, Y.; Gao, S.; Liu, W.; Wei, D. Effects of rare earth elements doping on gas sensing properties of ZnO nanowires. *Ceram. Int.* **2021**, *47*, 24218–24226. [CrossRef]

26. Yu, S.; Zhang, H.; Lin, C.; Bian, M. The enhancement of humidity sensing performance based on Eu-doped ZnO. *Curr. Appl. Phys.* **2019**, *19*, 82–88. [CrossRef]
27. Fu, X.Q.; Wang, C.; Yu, H.C.; Wang, Y.G.; Wang, T.H. Fast humidity sensors based on CeO_2 nanowires. *Nanotechnology* **2007**, *18*, 145503. [CrossRef]
28. Lyle, S.J.; Westall, W.A. A study of the thermal decomposition of hydrated europium (III) chloride and europium (III) bromide. *Thermochim. Acta* **1983**, *68*, 51–58. [CrossRef]
29. Jiang, W.; Bian, Z.; Hong, C.; Huang, C. A mild liquid reduction route toward uniform blue-emitting $EuCl_2$ nanoprisms and nanorods. *Inorg. Chem.* **2011**, *50*, 6862–6864. [CrossRef] [PubMed]
30. Shen, Z.; Zhang, G.; Zhou, H.; Sun, P.; Li, B.; Ding, D.; Xhen, T. Macroporous lanthanide-organic coordination polymer foams and their corresponding lanthanide oxides. *Adv. Mater.* **2008**, *20*, 984–988. [CrossRef]
31. Wang, S.; Wang, W.; Qian, Y. Preparation and characterization of Eu_2O_3 nanometer thin films by pulse ultrasonic spray pyrolysis method. *Mater. Res. Bull.* **2000**, *35*, 2057–2062. [CrossRef]
32. Buvailo, A.I.; Xing, Y.; Hines, J.; Dollahon, N.; Borguet, E. TiO_2/LiCl-based nanostructured thin film for humidity sensor applications. *ACS Appl. Mater. Interfaces* **2011**, *3*, 528–533. [CrossRef] [PubMed]
33. Wang, W.; Li, Z.; Liu, L.; Zhang, H.; Zheng, W.; Wang, Y.; Huang, H.; Wang, Z.; Wang, C. Humidity sensor based on LiCl-doped ZnO electrospun nanofibers. *Sens. Actuators B* **2009**, *141*, 404–409. [CrossRef]
34. Song, X.; Qi, Q.; Zhang, T.; Wang, C. A humidity sensor based on KCl-doped SnO_2 nanofibers. *Sens. Actuators B* **2009**, *138*, 368–373. [CrossRef]
35. Feng, C.D.; Sun, S.L.; Wang, H.; Segre, C.U.; Stetter, J.R. Humidity sensing properties of Nafion and sol−gel derived SiO_2/Nafion composite thin films, Sens. *Actuators B* **1997**, *40*, 217–222. [CrossRef]
36. Wang, J.; Lin, Q.; Zhang, T.; Zhou, R.; Xu, B. Humidity sensor based on composite material of nano-$BaTiO_3$ and polymer RMX. *Sens. Actuators B* **2002**, *81*, 248–253. [CrossRef]
37. Wang, J.; Xu, B.K.; Ruan, S.P.; Wang, S.P. Preparation and electrical properties of humidity sensing films of $BaTiO_3$/polystrene sulfonic sodium. *Mater. Chem. Phys.* **2003**, *78*, 746–750. [CrossRef]
38. Casalbore-Miceli, G.; Yang, M.J.; Camaioni, N.; Mari, C.M.; Li, Y.; Sun, H.; Ling, M. Investigations on the ion transport mechanism in conduction polymer films. *Solid State Ionics* **2000**, *131*, 311–321. [CrossRef]